Materials Advances

ROYAL SOCIETY OF CHEMISTRY

PAPER

View Article Online
View Journal | View Issue

Check for updates

Cite this: *Mater. Adv.*, 2022, 3, 8276

A novel biodegradable ureteral stent with antibacterial ability to inhibit biofilm formation

Kaiqi Li,[ab] Xiliang Liu,[ab] Xiangjie Di,[c] Yiliang Bao,[d] Yihong Bao,[d] Chengdong Xiong[a] and Dongliang Chen*[a]

Received 27th May 2022,
Accepted 1st September 2022

DOI: 10.1039/d2ma00593j

rsc.li/materials-advances

Biodegradability and surface modification such as hydrophilicity have been crucial for the design of materials for ureteral stents in recent years. To satisfy the above properties, more work has focused on imparting more functionalities, such as antibacterial properties, to the material. In this work, the influence and antibacterial effect of modification by blending with poly(L-lactide-*co*-5-amino-1,3-dioxan-2-one) (P(LA-*co*-AC)) on the structure and properties of poly(L-lactide-*co*-ε-caprolactone) (PLACL) were investigated. Modified biodegradable PLACL was confirmed to have good hydrophilicity which can resist protein adhesion, good biocompatibility and excellent antibacterial ability, which could not only inhibit bacterial biofilm formation but also kill free bacteria in the substrate. The tensile strength, anti-protein fouling and antibacterial properties were improved with the weight percentage of P(LA-*co*-AC), while the degradation rate of the PLACL substrate was accelerated. This work provides a new method to surmount the problems faced by urological surgery which comply with the future trend in biodegradable ureteral stent design.

Open Access Article. Published on 06 September 2022. Downloaded on 8/11/2025 4:44:09 AM.
This article is licensed under a Creative Commons Attribution-NonCommercial 3.0 Unported Licence.

Introduction

The ureteral stent is one of the most common surgical implants used after urological surgery, and aims to provide temporary urinary upper tract drainage and promote ureteral recovery.[1–4] Since Finney *et al.* designed the "Double J" ureteral stent in 1978,[5] it has been relatively stagnant in terms of engineering design, but has continued to innovate in terms of materials.[3,6–10]

For example, in order to avoid secondary surgical intervention, biodegradable ureteral stents have been widely studied.[7,11,12] Unlike non-degradable materials such as metal or silicone, biodegradable ureteral stents can be either natural or synthetic and can be eliminated *via* normal metabolic pathways. The U.S. Food and Drug Administration (FDA) has already confirmed polylactic (PLA), poly-ε-caprolactone (PCL), polytrimethylene carbonate (TMC) and their copolymers such as poly(L-lactide-*co*-ε-caprolactone) (PLACL) as biomaterials,[13] which can be used as surgical implants or in the field of tissue engineering.[14] As for ureteral stents, the material not only needs to have good biocompatibility, but also needs to be relatively flexible.[4,15] Our group has made a lot of progress in the field of biodegradable ureteral stents.[16–18] PLACL is a relatively successful material for the next generation of ureteral stents that can be synthesized into amorphous elastomers with good toughness and biodegradability.

Although ureteral stents have been a routine procedure in urological surgery for decades, many problems remain. Infection and encrustation were the main causes of stent failure in recent studies.[4,15,19] When infection occurs, encrustation becomes severe due to the urease-producing bacteria which elevate the pH of the urine, resulting in a reduction in the solubility of crystalline salts.[20] Therefore, it is critical to solve the problem of infection caused by bacteria. Microbial pathogens such as *Escherichia coli* (*E. coli*), *Proteus mirabilis*, and *Enterococcus faecalis* are ubiquitous in our urinary system, which seriously hinders the use of ureteral stents, even threatening human health.[21] In addition, when bacteria attach to the stent surfaces, they wrap themselves in a hydrated, self-secreted polymeric matrix, forming a biofilm.[22–25] This will be a breeding ground for bacteria to grow, keeping them away from conventional antibiotics and even evading host immune responses. As consequence, it is extremely challenging for researchers to surmount infection and bacterial biofilm formation.

Antibacterial or antibiofilm strategies for ureteral stents involving hydrogel coating, antibiotic coating or coating with antimicrobial agents are currently under investigation.[19,26–30] However, the disadvantage of the coating is obvious: that is, it easily fails with the degradation process. Therefore, we need to design a ureteral stent that can overcome the degradation process and be effectively antibacterial from beginning to end.

[a] *Chengdu Institute of Organic Chemistry, Chinese Academy of Sciences, Chengdu 610041, P. R. China. E-mail: dlchen@cioc.ac.cn*
[b] *University of Chinese Academy of Sciences, Beijing 100039, P. R. China*
[c] *Clinical Trial Center/NMPA Key Laboratory for Clinical Research and Evaluation of Innovative Drug, West China Hospital of Sichuan University, Chengdu 610041, P. R. China*
[d] *ZheJiang ZhongZai Medical Technology Co. Ltd, Zhejiang 322015, P. R. China*

© 2022 The Author(s). Published by the Royal Society of Chemistry

Open Access Article. Published on 06 September 2022. Downloaded on 8/11/2025 4:44:09 AM.
This article is licensed under a Creative Commons Attribution-NonCommercial 3.0 Unported Licence.

Obviously, this needs to be considered from the perspective of the material itself. According to the literature, increasing the hydrophilicity of the material can indirectly achieve the antibacterial effect, due to reducing the adhesion of proteins, and inhibiting the formation of the conditioning layer for bacteria to grow.[31–33] Our group previously evaluated a novel type of ureteral stent composed of methoxypoly(ethylene glycol)-*block*-poly(L-lactide-ran-ε-caprolactone) (mPEG-PLACL),[16] and the results provided useful information that the hydrophilic polymers were effective against protein adhesion and showed great promise as a commercially available urinary biomaterial. Further, we found that the introduction of bactericidal groups such as amino cations, can not only improve the hydrophilicity, but also directly endow the material with antibacterial properties.[34,35]

In this study, we synthesized a macromolecule with pendant primary amine groups, named poly (L-lactide-*co*-5-amino-1,3-dioxan-2-one) (P(LA-*co*-AC)), which mimicked antimicrobial peptides (AMP).[36] Based on reports in the literature, this AMP structure could attach to the microbial membrane *via* electrostatic attractions between their cationic groups and the surface of the anionic membrane. When this occurs, hydrophobic chains intercalate into the microbial membrane to induce membrane destabilization and subsequent leakage of cytoplasmic content, leading to lysis. Blending this AMP-mimicking P(LA-*co*-AC) with the matrix PLACL in a certain proportion, a novel biodegradable ureteral stent with antibacterial ability was prepared. Compared to some polyhydroxy acid copolymers with amino side-chain groups, P(LA-*co*-AC) and PLACL have good compatibility due to the LA segment as the main body in their chains, so they can be mixed homogeneously without destroying the mechanical property. The antibacterial properties of the stent against *Escherichia coli* were characterized, and it was found that it could not only inhibit the adhesion of bacteria on the surface, but also effectively kill the bacteria in the medium, due to the diffusion of small molecular segments of the cationic polymer during the degradation process. In addition, the stent still has good biocompatibility (cytotoxicity). The effects of hydrophilicity, anti-protein fouling, as well as the mechanical properties and degradation properties *in vitro* were also studied.

Material and methods

Materials

L-Lactide (LA) was purchased from Huizhou Foryou Medical Devices Co. Ltd. ε-caprolactone and stannous octoate (Sn (Oct)$_2$) were purchased from Sigma-Aldrich (U.S.A). Other chemical products were purchased from Aladdin, and used as received.

Polymer synthesis

Synthesis of P(LA-*co*-AC). The ring-opening polymerization (ROP) of L-LA and 5-((2-nitrobenzyl) amino)-1,3-dioxan-2-one (NBAC) with specified molar ratios was carried out in bulk at 120 °C, with Sn (Oct)$_2$ as catalyst. A mass ratio of LA + NBAC *versus* Sn (Oct)$_2$ of 1000 was applied. The reaction was terminated by cooling the flask to room temperature. The polymer was dissolved in dichloromethane (DCM), precipitated by an amount of ethanol, and isolated by filtration. The protected copolymer P(LA-*co*-NBAC) was dissolved in $CHCl_3$, and the solution was stirred under a specific UV lamp (365 nm, 20 mW cm^{-}2) for 10 h. Then a large amount of ethanol/petroleum ether was dropped into the polymer solution to precipitate the deprotected polymer P(LA-*co*-AC) with free pendant amino groups. The synthesis process is shown in Scheme 1. From our previous work, P(LA-*co*-AC) stands for P(LA-*co*-10% AC) in this study, due to its suitable molecular weight and degree of functionalization.

Synthesis of PLACL. PLACL was synthesized by ROP under vacuum at 140 °C for 72 h using Sn (Oct)$_2$ as the catalyst. The copolymer was purified by dissolution in DCM and precipitation into ethanol, washed with fresh ethanol, and dried at room temperature under vacuum. The synthesis process is shown in Scheme 2. From our previous work, PLACL stands for P(75% LA-*ran*-25% ε-CL) in this study, due to its suitable mechanical strength and degradation rate.

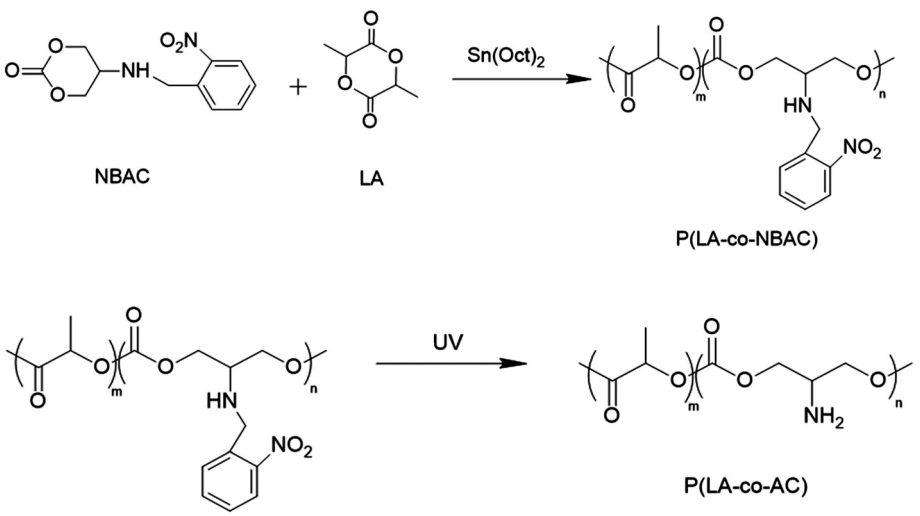

Scheme 1 Synthesis of poly(L-lactide-*co*-5-amino-1,3-dioxan-2-one).

Open Access Article. Published on 06 September 2022. Downloaded on 8/11/2025 4:44:09 AM.
This article is licensed under a Creative Commons Attribution-NonCommercial 3.0 Unported Licence.

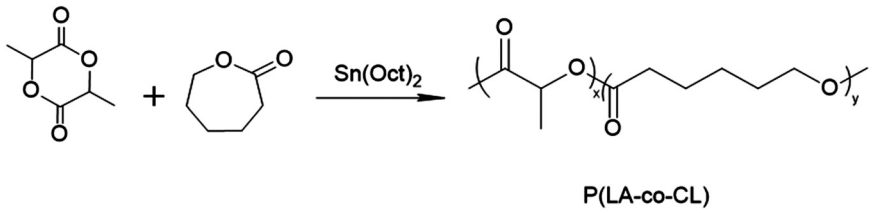

Scheme 2 Synthesis of poly(L-lactide-*ran*-ε-caprolactone) (PLACL).

Preparation of polymer blending

Specified mass ratios of P(LA-*co*-AC) and PLACL were dissolved in DCM and precipitated with an amount of ethanol, washed with fresh ethanol, and isolated by filtration. Here, 5%, 10%, and 20% mass ratios of P(LA-*co*-AC) were selected for blending with PLACL. The purified blends were compression-molded at 150 °C using 4 mm thick stainless steel molds using an XLB press plate vulcanizer (Haimen Jinma, China).

Mechanical properties

All mechanical tests were performed on compression-molded films. The tensile tests were carried out on a Model CMT 4503 type SANS tensile tester (China) with a drawing speed of 100 mm min^{-1} at 25 °C. All samples were cut into 50 mm × 5 mm and immobilized between fixings. The tensile strength and extension at break were obtained from the stress–strain diagram. Each reported value was the mean and standard deviation of three parallel samples.

Degradation properties

All samples were selected for both artificial urine (Table 1) and deionized water degradation *in vitro* and degraded for 40 days at a constant temperature of 37 °C. The ratio of artificial urine to sample was 50 : 1 (v/w, mL g^{-1}). The dimensions of the samples were the same as those in the mechanical test. The samples were divided into five groups corresponding to 5D, 10D, 20D, 30D and 40D, respectively, with three parallel samples per set. The weight loss ratio was calculated according to eqn (1):

$$\text{Weight loss}(\%) = \frac{W_0 - W_{\text{dry}}}{W_0} \quad (1)$$

where W_0 is the original dry weight of the sample and W_{dry} is the dry weight of the sample after degradation for different periods.

Table 1 Artificial urine for degradation

Reagent	Concentration (g L^{-1})
$CaCl_2 \cdot 2H_2O$	0.65
$MgCl_2 \cdot 6H_2O$	0.65
NaCl	4.60
Na_2SO_4	2.30
KCl	1.60
NH_4Cl	1.00
KH_2PO_4	2.80
Sodium citrate-dihydrate	0.65
Sodium oxalate	0.02
Urea	25.0
Creatinine	1.10

Water contact angle (WCA) and anti-protein adsorption performance analysis

After the water droplet had been in contact with the sample for 30 s, the water contact angle was measured on the air surface of the sample at 25 ± 0.5 °C using a contact angle system (JC2000D1, Shanghai, China).

In order to evaluate the anti-protein adsorption performance of the stent surface, the Coomassie blue staining (Bradford) method was carried out. First, different concentrations of bovine serum albumin (BSA) (20–100 μg mL^{-1})/PBS solution were mixed with Coomassie blue (G-250), and an ultraviolet-visible spectrophotometer was used to measure the absorbance of the solution at 595 nm to draw a protein (BSA) adsorption standard curve. After that, BSA/PBS solution with a 50 μg mL^{-1} concentration was prepared to immerse and incubate the samples for 4 h, 8 h, 16 h, 24 h, and 48 h. The dimensions of the samples were the same as those in the mechanical test. At each time point, a certain volume of BSA/PBS solution was taken out and mixed with Coomassie blue; then the UV spectrophotometer was used to measure the absorbance. The concentration could be calculated from the standard curve. The results were calculated according to Equation (2):

$$M_{\text{ads}} = V \times (c_0 - c) \quad (2)$$

where c_0 (mg mL^{-1}) is the concentration of the solute without immersion of sample, c (mg mL^{-1}) is the concentration of the solute in the BSA/PBS solution after adsorption at each time point, and $V(L)$ is the volume of the BSA/PBS solution.

Assessment of antibacterial performance of ureteral stents

Escherichia coli was selected for this assessment, and this test was divided into two parts. The first part was bacteriostasis (preventing bacteria from adhering to the surface of the material), and the second was the bactericidal effect (killing of bacteria in the medium by the material). 1 mL of Luria–Bertani (LB) medium was added to bacterial suspension, and cultivated at 37 °C for 24 h. Then LB medium was used to dilute the bacterial solution 10^6 times. All samples were immersed in 1 mL of bacterial solution and cultured at 37 °C for 48 h.

(a) After the sample was taken out, it was immersed in sterile PBS solution 3 times to remove non-adherent bacteria. Finally, the adhered bacteria were eluted from the surface by 40 kHz sonication into 1 mL of sterile LB, and plated to count the colony.

(b) A 50 μL diluted bacterial suspension was inoculated in a plate of LB-agar medium, and the colony count of each

© 2022 The Author(s). Published by the Royal Society of Chemistry

Open Access Article. Published on 06 September 2022. Downloaded on 8/11/2025 4:44:09 AM.
This article is licensed under a Creative Commons Attribution-NonCommercial 3.0 Unported Licence.

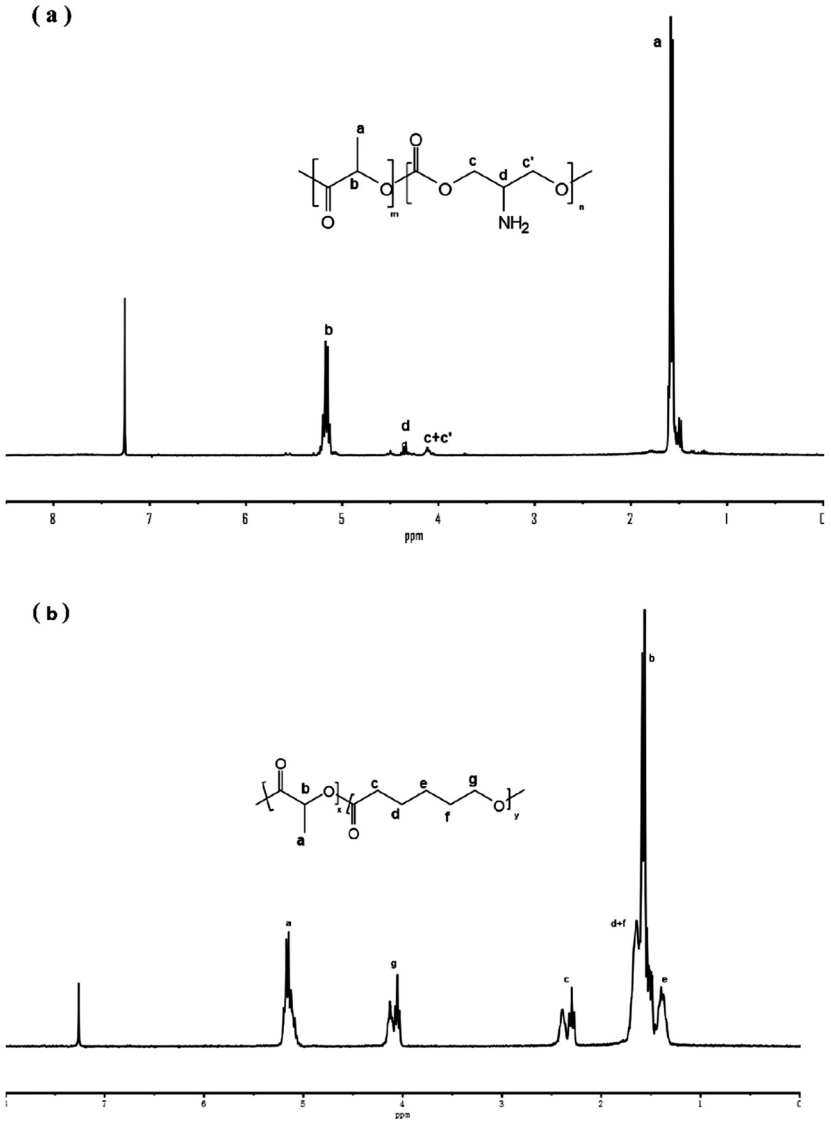

Fig. 1 ^{1}H NMR spectra of (a) P(LA-*co*-AC) and (b) PLACL.

bacterial sample formed on the LB-agar plate was determined after 24 h of incubation at 37 °C.

Results and discussion

^{1}H NMR analysis

Fig. 1 shows the ^{1}H NMR spectra of copolymer P(LA-*co*-AC) and PLACL. 5%, 10%, and 20% mass ratios of P(LA-*co*-AC) were selected to blend with PLACL. The molecular weight data are shown in Table 2.

Table 2 Molecular weight data of P(LA-*co*-AC)[a] and PLACL[b]

Polymer	M_n (10^4)[c]	M_w (10^4)[c]	M_w/M_n[c]
P(LA-*co*-AC)	1.74	2.23	1.23
PLACL	10.1	20.9	2.07

[a] P(LA-*co*-AC) stands for P(LA-*co*-10% AC). [b] PLACL stands for P(75% LA-*ran*-25% ε-CL). [c] Apparent molecular weight determined by GPC ($CHCl_3$ as eluent).

Tensile strength

The tensile strength and extension at break of samples with different blends of components are shown in Fig. 2. With an increase in blending ratio, the tensile strength and extension at break showed opposite trends. Tensile strength is positively correlated with the proportion of P(LA-*co*-AC). In the 20% P(LA-*co*-AC) group, the tensile strength reached 15.6 MPa, a 25% increase compared to the control PLACL. The amino is a polar group, which enhances the interaction force between the molecular chains. As a result, the tensile strength increases at the macro level. However, due to the enhanced intermolecular force, the relative slippage of the molecular chains becomes difficult and the extension at break decreases. At 5%, 10% and 20% blending contents, the extension at break of the material decreased by 18%, 9% and 25%, respectively.

Open Access Article. Published on 06 September 2022. Downloaded on 8/11/2025 4:44:09 AM.
This article is licensed under a Creative Commons Attribution-NonCommercial 3.0 Unported Licence.

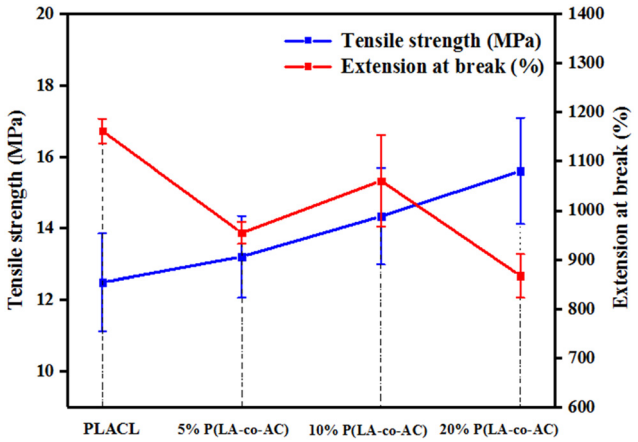

Fig. 2 The results of tensile strength and extension at break.

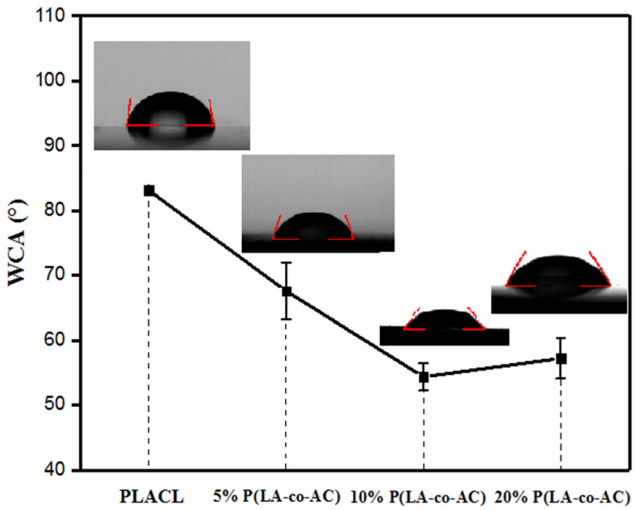

Fig. 3 Water contact angle of the blends.

Water contact angle (WCA) and anti-protein adsorption performance analysis

In order to measure the influence of different components of P(LA-*co*-AC) on the hydrophilicity of the material, water contact angle measurements were carried out and are shown in Fig. 3. In the groups with 10% and 20% P(LA-*co*-AC), the contact angles dropped below 60°, and a drop of more than 20° compared with PLACL strongly demonstrated an enhancement in hydrophilicity. The 20% P(LA-*co*-AC) group has more amino groups than the 10% P(LA-*co*-AC) group, due to the saturation of the functional groups exposed to the air at the interface and the enhanced non-covalent bonding between the amino groups, so the interaction with water may be reduced, resulting in the phenomenon where the contact angles are not significantly reduced but are slightly increased.

Amino as a polar group can effectively improve the hydrophilicity of the polymer chains and form a hydration layer against protein adhesion. Previous studies have shown that the hydration layer formed by cationic polymer through the strong hydration of the ions is superior to that of the PEG chains, so it can have higher anti-protein fouling performance. When the protein content is in the range of 0–1000 μg mL^{-1}, the absorbance of the BSA-Coomassie blue complex at 595 nm is proportional to the concentration. The standard adsorption curve of BSA concentration and absorbance is shown in Fig. 4(a). As shown in Fig. 4(b), the group with 20% P(LA-*co*-AC) has better anti-protein adhesion property, which was reduced by over 50% compared to the control PLACL. Adsorption of the protein increased significantly within 12–24 hours, but moderated after 24 hours, nearly reaching adsorption equilibrium.

Degradation properties

In artificial urine formula, the concentration of inorganic salts is quite high, leading to deposition and encrustation on the surface of materials during degradation, which is why the weight loss can be negative in Fig. 5(a). Therefore, deionized water was used for degradation to compare with artificial urine

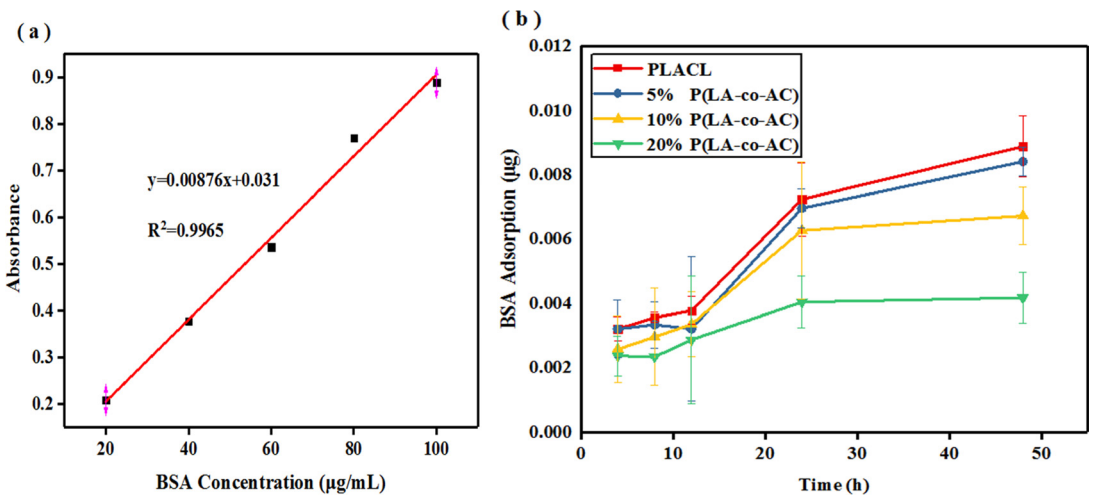

Fig. 4 Anti-protein adsorption performance analysis: (a) BSA adsorption standard curve; (b) protein adsorption behavior.

© 2022 The Author(s). Published by the Royal Society of Chemistry

Open Access Article. Published on 06 September 2022. Downloaded on 8/11/2025 4:44:09 AM.
This article is licensed under a Creative Commons Attribution-NonCommercial 3.0 Unported Licence.

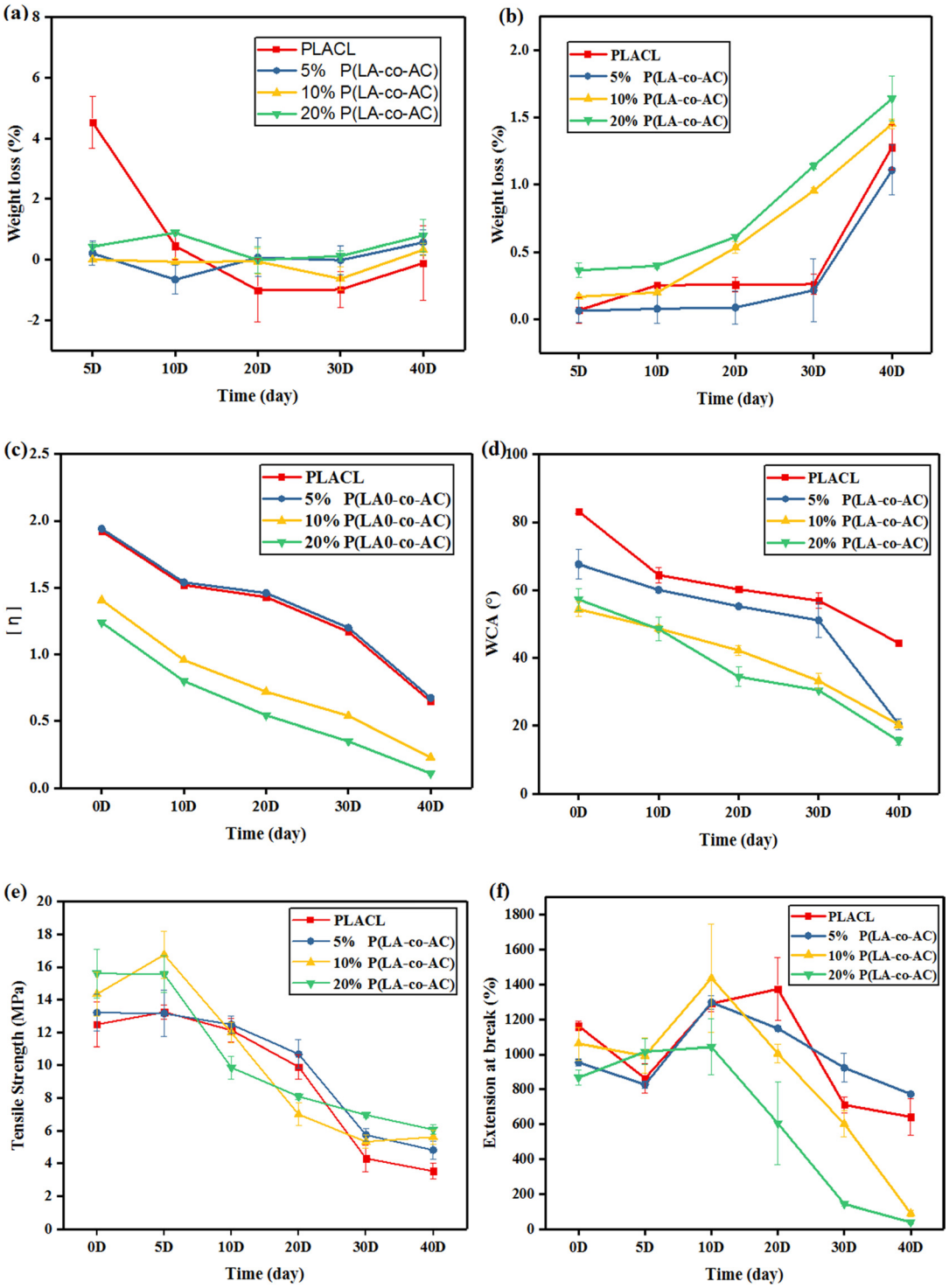

Fig. 5 Degradation properties: (a) weight loss in artificial urine; (b) weight loss in deionized water; (c) intrinsic viscosity; (d) WCA change; (e) tensile strength; and (f) extension at break.

in weight loss of the samples. Apart from weight loss, the rest of the data reflected the degradation process in artificial urine. From Fig. 5(a) and (b), it can be seen that the weight loss of the samples within 40 days is not significant. A relatively high (around 4.5%) weight loss of PLACL in 5 day degradation in artificial urine may be due to the diffusion of small molecular chains in the material, and the fact that the weight loss was not obvious in the blended groups may be due to the increased intermolecular force making it difficult for small segments to diffuse out. Blending with P(LA-*co*-AC) resulted in higher weight loss in deionized water, but only up to 1.5% in the 20% P(LA-*co*-AC) group.

Open Access Article. Published on 06 September 2022. Downloaded on 8/11/2025 4:44:09 AM.
This article is licensed under a Creative Commons Attribution-NonCommercial 3.0 Unported Licence.

After blending with P(LA-*co*-AC), the intrinsic viscosity of the material decreased in Fig. 5(c). In the groups with 10% and 20% P(LA-*co*-AC), the intrinsic viscosity decreased by 0.58 and 0.61, respectively, compared with PLACL. Due to the low molecular weight of P(LA-*co*-AC), it could act as a plasticizer after blending with PLACL, so the flow time is shortened and the intrinsic viscosity of the material is reduced. After 40 days of degradation *in vitro*, the intrinsic viscosities of PLACL, 5% P(LA-*co*-AC), 10% P(LA-*co*-AC) and 20% P(LA-*co*-AC) decreased by 1.27, 1.27, 1.18 and 1.13, respectively, and the significant decrease in intrinsic viscosity reflected the rapid degradation process of the material. The above results indicate that the degradation of PLACL and its blends occurred in the form of bulk degradation, which is why the weight losses were not obvious but the molecular weight dropped sharply.

Using the water contact angle (WCA) to characterize the change in the hydrophilicity of the material can also reflect the degradation process. Degradation could generate a large number of polar end groups, such as carboxyl, improving the hydrophilicity of the surface. In Fig. 5(d), after 40 days of degradation *in vitro*, the contact angles of PLACL, 5% P(LA-*co*-AC), 10% P(LA-*co*-AC) and 20% P(LA-*co*-AC) decreased by 38.7°, 47.1°, 34.09° and 41.67°, respectively, and the changes in hydrophilicity also reflected the process of rapid degradation. Among them, the contact angle results of the 5% P(LA-*co*-AC) and 20% P(LA-*co*-AC) groups decreased by more than 40°, indicating that the blending of P(LA-*co*-AC) had a huge impact on the

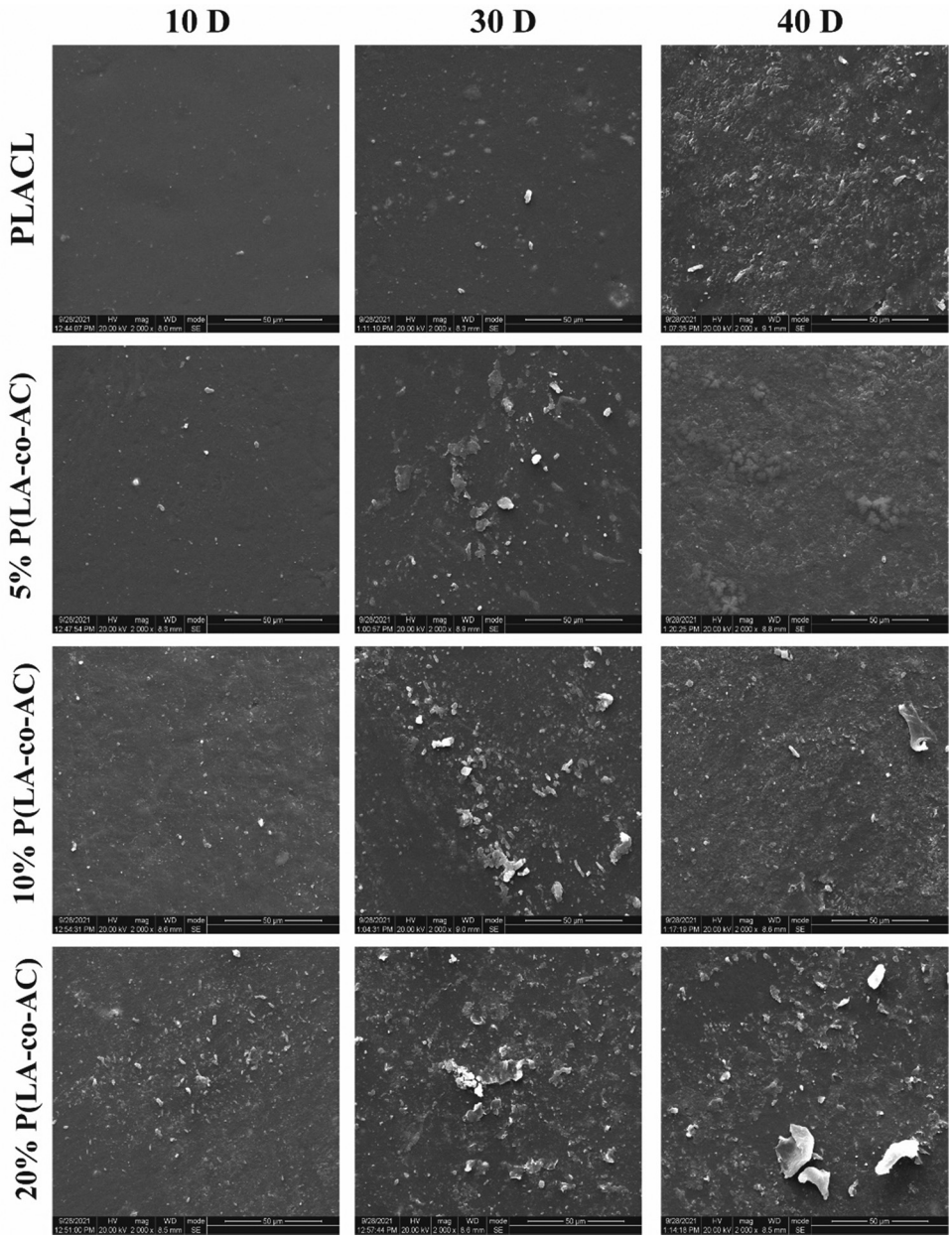

Fig. 6 SEM micrographs of sample surfaces in different degradation periods.

 © 2022 The Author(s). Published by the Royal Society of Chemistry

Open Access Article. Published on 06 September 2022. Downloaded on 8/11/2025 4:44:09 AM.
This article is licensed under a Creative Commons Attribution-NonCommercial 3.0 Unported Licence.

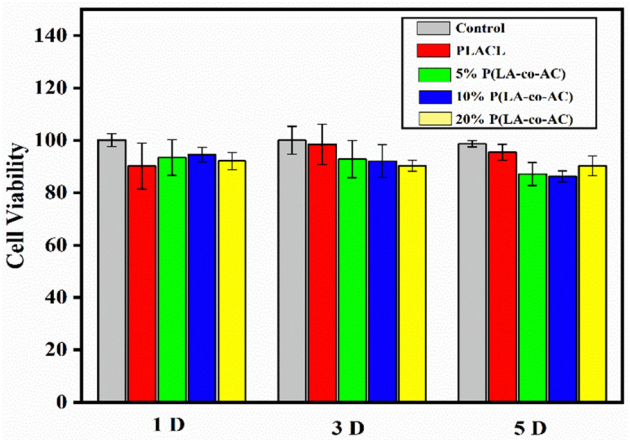

Fig. 7 Cell viability test of samples by CKK-8 assay.

degradation process, so there is a tendency to accelerate degradation.

Fig. 5(e) and (f) characterize the changes in mechanical properties during degradation. At the end of degradation, the tensile strengths of PLACL, 5% P(LA-*co*-AC), 10% P(LA-*co*-AC) and 20% P(LA-*co*-AC) were reduced by 72%, 64%, 61%, and 61%, respectively. And after 40 days of degradation, the tensile strengths of the blends were still higher than that of PLACL. The degradation trends reflected by the tensile strengths were basically the same as before, but the extension at break at around 10 days of degradation increased to a certain extent. After ten days of immersion in artificial urine, large amounts of water entered into the materials and interacted with the molecular chains, which may enhance the toughness. In addition, the samples may also spontaneously undergo an annealing-like process in which the molecular chains are stretched and the extensions at break are enhanced. It was found that, although the blending of P(LA-*co*-AC) improved the tensile strength, it accelerated the embrittlement of the material during the degradation process. At the end of degradation, the extension at break of 20% P(LA-*co*-AC) was reduced by 95%, while that of PLACL decreased by only 45%. Therefore, from the point of view of mechanical properties, it is not the case that the higher the ratio of P(LA-*co*-AC), the better.

SEM micrographs of the sample surfaces in different degradation periods are shown in Fig. 6, reflecting the surface morphologies at different periods. As the degradation time increased, the inorganic salts in the artificial urine would be precipitated, and these substances would interact with the surface. The blended groups contained more polar groups, so

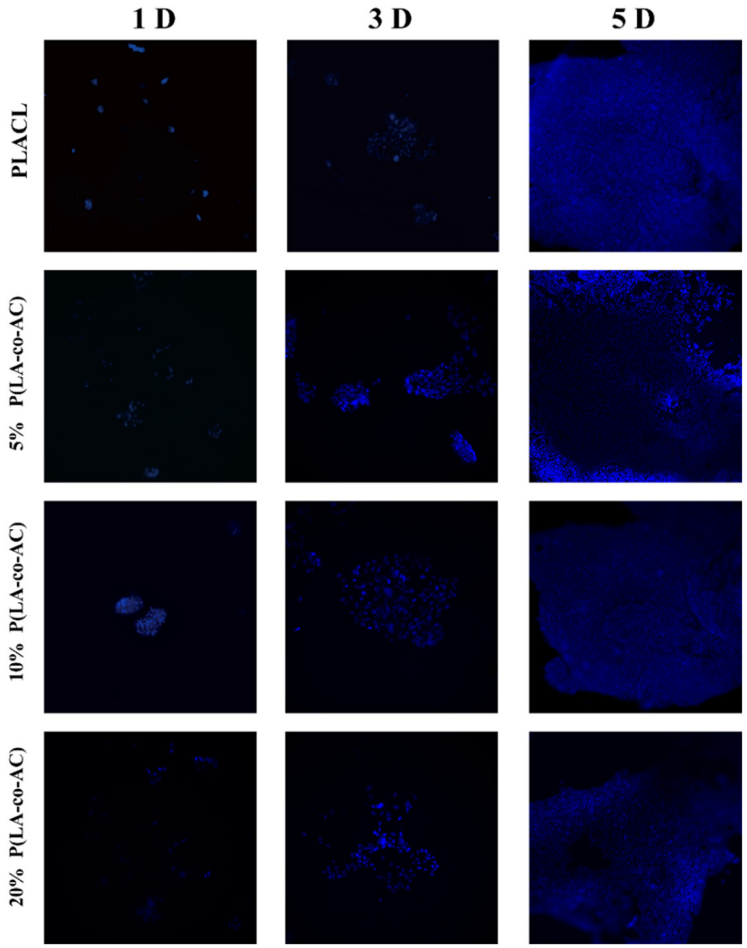

Fig. 8 Fluorescence microscopy of the samples on HEK-293 cells.

Open Access Article. Published on 06 September 2022. Downloaded on 8/11/2025 4:44:09 AM.
This article is licensed under a Creative Commons Attribution-NonCommercial 3.0 Unported Licence.

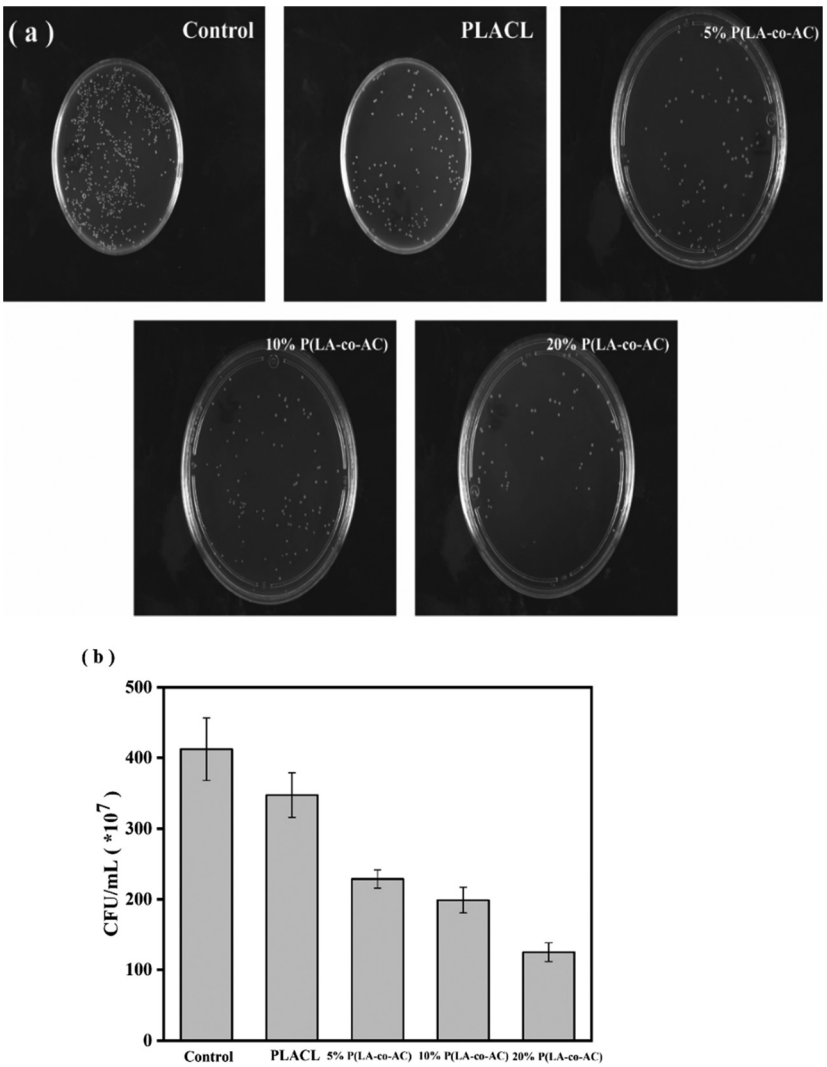

Fig. 9 Assessment of the bacteriostasis properties: (a) photographs of *E. coli* colonies; (b) colony counts.

the surfaces were more likely to produce crystals. Therefore, from the perspective of anti-encrustation, it is not the case that the higher the ratio of P(LA-*co*-AC), the better. At the same time, there was no obvious corrosion on the surface of the samples, which also proved that the material did not undergo surface degradation.

Cytotoxicity

As an implant material, it should have good biocompatibility, and human embryonic kidney cells (HEK-293) were used to assess the cytotoxicity of the samples. A 96-well plate (5000 cells per well) was used and all samples in the cells were incubated at 37 °C with 5% CO_2 for 1 d, 3 d, and 5 d. Cytotoxicity was assessed by a CKK-8 assay and fluorescence microscopy (Nikon Ti E), as shown in Fig. 7 and 8. No significant negative effects on cell growth were observed with the blends. The CKK8 assay showed that cell viability in each group was over 85% and more fluorescence was observed on the surface, indicating that cell proliferation was enhanced on the fifth day, proving that the material has good biocompatibility and is suitable for ureteral stents.

Assessment of antibacterial performance

The antibacterial property was tested against *E. coli*, a common bacterium when urinary tract infections occur. The bacteriostasis properties (preventing bacteria from adhering to the surface of the material) are shown in Fig. 9, and the results of the bactericidal effect (killing of bacteria in the medium by the material) are shown in Fig. 10.

When bacteria attach to the stent surface, they will secrete a polymeric matrix and form a biofilm to protect themselves. Therefore, reducing the adsorption of proteins and adhesion of bacteria will effectively inhibit the formation of biofilms. Resistance to protein adsorption has been demonstrated previously, and the role of cationic polymers in preventing bacterial adhesion will be demonstrated here. In Fig. 9, an enhancement in the antibacterial performance with increased content of P(LA-*co*-AC) was observed. Compared with PLACL, the bacteriostatic effect of the 20% P(LA-*co*-AC) group was approximately three times greater, which proved its excellent bacteriostatic performance.

As a degradable material, the amino-cation polymer fragments will diffuse into the medium with the degradation

 © 2022 The Author(s). Published by the Royal Society of Chemistry

Open Access Article. Published on 06 September 2022. Downloaded on 8/11/2025 4:44:09 AM.
This article is licensed under a Creative Commons Attribution-NonCommercial 3.0 Unported Licence.

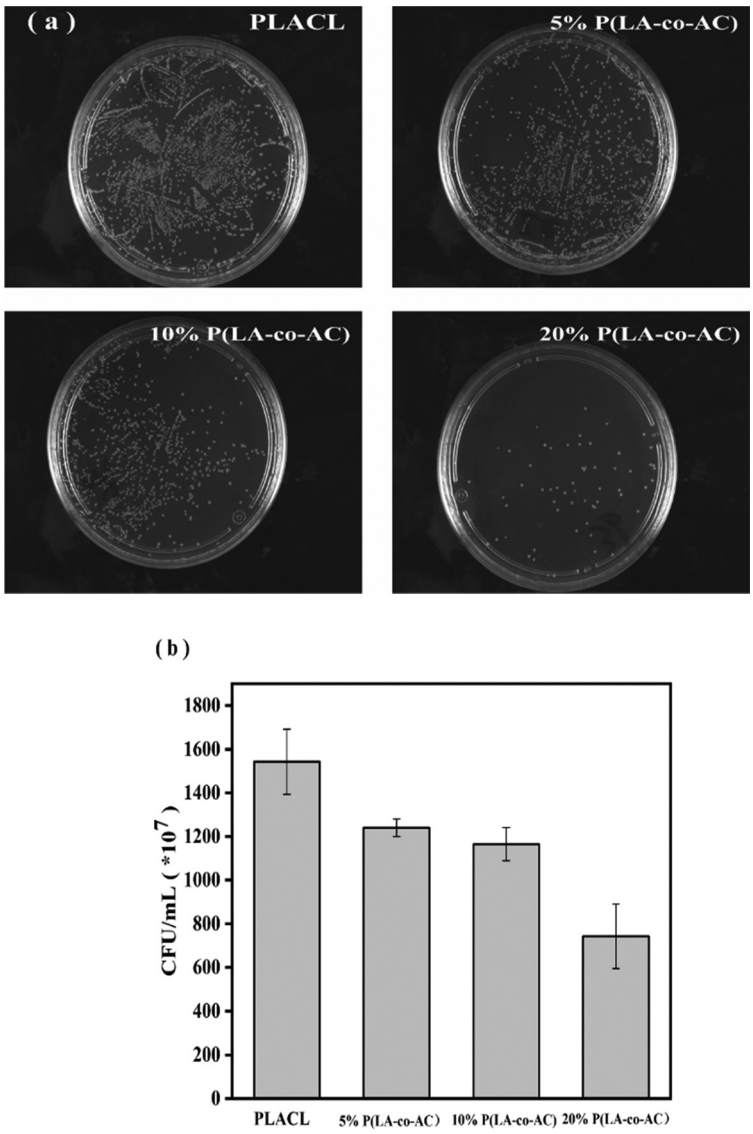

Fig. 10 Assessment of the bactericidal effect: (a) photographs of *E. coli* colonies; (b) colony counts.

process, and this AMP-like structure will have a bactericidal effect. These hydrophilic–hydrophobic chains can interact with bacteria through electrostatic attraction, disrupting the bacterial membrane and killing it. By culturing the bacterial suspension of the cultured samples, it is found that the number of colonies of *E. coli* decreased significantly with an increase in P(LA-*co*-AC) content in the samples. This novel ureteral stent material with both antibacterial and bactericidal effects can not only effectively inhibit the formation of biofilms, but also solve infections caused by bacteria to a certain extent.

Conclusion

A PLA-copolymer, named P(LA-*co*-AC), with primary amine groups was successfully synthesized by ring-opening polymerization, which not only improved the hydrophilicity of the chains, but also endowed the polymer with antibacterial properties. By blending this polymer with PLACL, a novel biodegradable material was prepared with antibacterial ability which inhibits biofilm formation and can be used for ureteral stents. By studying its mechanical properties, anti-protein adsorption performance, degradation properties, biocompatibility and antibacterial properties, the material showed it will have great potential in the field of biodegradable ureteral stents.

Data availability statement

The data that support the findings of this study are available on request from the corresponding author. The data are not publicly available due to privacy or ethical restrictions.

Conflicts of interest

There are no conflicts to declare.

Open Access Article. Published on 06 September 2022. Downloaded on 8/11/2025 4:44:09 AM. This article is licensed under a Creative Commons Attribution-NonCommercial 3.0 Unported Licence.

Acknowledgements

This work would like to appreciate Zhejiang ZhongZai Medical Technology Co.Ltd and Qian Fu from Shiyanjia Lab (www.shiyanjia.com) for some materials characterizations.

References

1 N. Venkatesan and K. Jayachandran, Polymers as Ureteral Stents, *J. Endourol.*, 2009, **24**, 191–198.
2 H. Brotherhood, D. Lange and B. H. Chew, Advances in ureteral stents, *Transl Androl Urol.*, 2014, 2223–4683.
3 C. Janssen, D. Lange and B. H. Chew, Ureteral stents – future developments, *Br. J. Med. Surg. Urol.*, 2012, **5**, S11–S17.
4 B. H. Chew and J. D. Denstedt, Technology Insight: novel ureteral stent materials and designs, *Nat. Clin. Pract. Urol.*, 2004, **1**(1), 44–48.
5 R. P. Finney, Experience with New Double J Ureteral Catheter Stent, *J. Urol.*, 1978, **120**(6), 678–681.
6 T. R. Yeazel and M. L. Becker, Advancing Toward 3D Printing of Bioresorbable Shape Memory Polymer Stents, *Biomacromolecules*, 2020, **21**(10), 3957–3965.
7 L. Wang, G. Yang, H. Xie and F. Chen, Prospects for the research and application of biodegradable ureteral stents: from bench to bedside, *J. Biomater. Sci., Polym. Ed.*, 2018, **29**(14), 1657–1666.
8 K. Hendlin, E. Korman and M. Monga, New metallic ureteral stents: improved tensile strength and resistance to extrinsic compression, *J. Endourol.*, 2012, **26**(3), 271–274.
9 R. N. Pedro, K. Hendlin, C. Kriedberg and M. Monga, Wire-based ureteral stents: impact on tensile strength and compression, *Urology*, 2007, **70**(6), 1057–1059.
10 H. C. L. L. pez-Huertas, A. J. Polcari, A.-M. Alex and T. M. T. Turk, Metallic Ureteral Stents: A Cost-Effective Method of Managing Benign Upper Tract Obstruction, *J Endourol.*, 2010, **24**, 483–485.
11 B. H. Chew, R. F. Paterson, K. W. Clinkscales, B. S. Levine, S. W. Shalaby and D. Lange, In vivo evaluation of the third generation biodegradable stent: a novel approach to avoiding the forgotten stent syndrome, *J. Urol.*, 2013, **189**(2), 719–725.
12 W. J. Fu, Z. X. Wang, G. Li, F. Z. Cui, Y. Zhang and X. Zhang, Comparison of a biodegradable ureteral stent versus the traditional double-J stent for the treatment of ureteral injury: an experimental study, *Biomed. Mater.*, 2012, **7**(6), 065002.
13 R. X. Qiu, C. M. Li, L. Ye, J. D. Dong, A. Y. Zhang, Y. Q. Gu and Z. G. Feng, Electrospinning of synthesized triblock copolymers of epsilon-caprolactone and L-lactide for the application of vascular tissue engineering, *Biomed. Mater.*, 2009, **4**(4), 044105.
14 A. Petas, M. Talja, T. L. J. Tammela, K. Taari, T. Valimaa and P. Tormala, The biodegradable self-reinforced poly-dl-lactic acid spiral stent compared with a suprapubic catheter in the treatment of post-operative urinary retention after visual laser ablation of the prostate, *Br. J. Urol.*, 1997, **80**(3), 439–443.
15 H. Rebl, J. Renner, W. Kram, A. Springer, N. Fritsch, H. Hansmann, O. W. Hakenberg and J. B. Nebe, Prevention of Encrustation on Ureteral Stents: Which Surface Parameters Provide Guidance for the Development of Novel Stent Materials?, *Polymers*, 2020, **12**(3), 558.
16 Y. Zhang, J. He, H. Chen and C. Xiong, A new hydrophilic biodegradable ureteral stent restrain encrustation both in vitro and in vivo, *J. Biomater. Appl.*, 2020, **35**(6), 720–731.
17 X. Liu, S. Liu, K. Li, Y. Fan, S. Feng, L. Peng, T. Zhang, X. Wang, D. Chen, C. Xiong, W. Bai and L. Zhang, Preparation and property evaluation of biodegradable elastomeric PTMC/PLCL networks used as ureteral stents, *Colloids Surf., A*, 2021, **630**, 127550.
18 X. Liu, S. Liu, Y. Fan, J. Qi, X. Wang, W. Bai, D. Chen, C. Xiong and L. Zhang, Biodegradable cross-linked poly(L-lactide-co-ε-caprolactone) networks for ureteral stent formed by gamma irradiation under vacuum, *J. Ind. Eng. Chem.*, 2021, **104**, 73–84.
19 C. M. Cottone, S. Lu, Y. X. Wu, K. Guan, R. Yoon, L. Limfueco, T. Hoang, W. Ciridon, B. D. Ratner, K. R. Johnson, R. M. Patel, J. Landman and R. V. Clayman, Surface-Treated Pellethanes: Comparative Quantification of Encrustation in Artificial Urine Solution, *J. Endourol.*, 2020, **34**(8), 868–873.
20 J. W. Warren, H. L. Jr., Muncie, J. R. Hebel and M. Hall-Craggs, Long-Term Urethral Catheterization Increases Risk of Chronic Pyelonephritis and Renal Inflammation, *J. Am. Geriatr. Soc.*, 1994, **42**(12), 1286–1290.
21 T. Cao, H. Tang, X. Liang, A. Wang, G. W. Auner, S. O. Salley and K. Y. Ng, Nanoscale investigation on adhesion of E. coli to surface modified silicone using atomic force microscopy, *Biotechnol. Bioeng.*, 2006, **94**(1), 167–176.
22 D. S. Uppu, S. Samaddar, C. Ghosh, K. Paramanandham, B. R. Shome and J. Haldar, Amide side chain amphiphilic polymers disrupt surface established bacterial bio-films and protect mice from chronic Acinetobacter baumannii infection, *Biomaterials*, 2016, **74**, 131–143.
23 E. F. Haney, Y. Brito-Sanchez, M. J. Trimble, S. C. Mansour, A. Cherkasov and R. E. W. Hancock, Computer-aided Discovery of Peptides that Specifically Attack Bacterial Biofilms, *Sci. Rep.*, 2018, **8**(1), 1871.
24 C. de la Fuente-Nunez, V. Korolik, M. Bains, U. Nguyen, E. B. Breidenstein, S. Horsman, S. Lewenza, L. Burrows and R. E. Hancock, Inhibition of bacterial biofilm formation and swarming motility by a small synthetic cationic peptide, *Antimicrob. Agents Chemother.*, 2012, **56**(5), 2696–2704.
25 J. W. Costerton, P. S. Stewart and E. P. Greenberg, Bacterial biofilms: a common cause of persistent infections, *Science*, 1999, **284**(5418), 1318–1322.
26 F. Cauda, V. Cauda, C. Fiori, B. Onida and E. Garrone, Heparin coating on ureteral Double J stents prevents encrustations: an in vivo case study, *J. Endourol.*, 2008, **22**(3), 465–472.
27 A. A. Barros, S. Browne, C. Oliveira, E. Lima, A. R. Duarte, K. E. Healy and R. L. Reis, Drug-eluting biodegradable ureteral stent: New approach for urothelial tumors of upper urinary tract cancer, *Int. J. Pharm.*, 2016, **513**(1-2), 227–237.
28 J. P. K. Tan, D. J. Coady, H. Sardon, A. Yuen, S. Gao, S. W. Lim, Z. C. Liang, E. W. Tan, S. Venkataraman, A. C. Engler,

 © 2022 The Author(s). Published by the Royal Society of Chemistry

Open Access Article. Published on 06 September 2022. Downloaded on 8/11/2025 4:44:09 AM.
This article is licensed under a Creative Commons Attribution-NonCommercial 3.0 Unported Licence.

M. Fevre, R. Ono, Y. Y. Yang and J. L. Hedrick, Broad Spectrum Macromolecular Antimicrobials with Biofilm Disruption Capability and In Vivo Efficacy, *Adv. Healthcare Mater.*, 2017, **6**(16), DOI: 10.1002/adhm.201601420.

29 C. R. Riedl, M. Witkowski, E. Plas and H. Pflueger, Heparin coating reduces encrustation of ureteral stents: a preliminary report, *Int. J. Antimicrob. Agents*, 2002, **19**, 507–510.

30 D. Minardi, O. Cirioni, R. Ghiselli, C. Silvestri, F. Mocchegiani, E. Gabrielli, G. d'Anzeo, A. Conti, F. Orlando, M. Rimini, L. Brescini, M. Guerrieri, A. Giacometti and G. Muzzonigro, Efficacy of tigecycline and rifampin alone and in combination against Enterococcus faecalis biofilm infection in a rat model of ureteral stent, *J. Surg. Res.*, 2012, **176**(1), 1–6.

31 N. Berna, P. Berna and S. Oscarsson, Polyol-promoted adsorption of serum proteins to amphiphilic agarose-based adsorbents, *J. Chromatogr. A*, 1997, **764**, 193–200.

32 Z. An, Y. Li, R. Xu, F. Dai, Y. Zhao and L. Chen, New insights in poly(vinylidene fluoride) (PVDF) membrane hemocompatibility: Synergistic effect of PVDF-g-(acryloyl morpholine) and PVDF-g-(poly(acrylic acid)-argatroban) copolymers, *Appl. Surf. Sci.*, 2018, **457**, 170–178.

33 X. Yan, C. Zhu, J. Huang, D. Qi and J. Li, Synthesis of Betaine Copolymer for Surface Modification of Cotton Fabric by Enhancing Temperature-Sensitive and Anti-Protein Specific Absorption Performance, *Materials*, 2021, **14**(22), 6793.

34 P. Song, Y. Shang, S. Chong, X. Zhu, H. Xu and Y. Xiong, Synthesis and characterization of amino-functionalized poly(propylene carbonate), *RSC Adv.*, 2015, **5**(41), 32092–32095.

35 P. G. Parzuchowski, A. Świderska, M. Roguszewska, T. Frączkowski and M. Tryznowski, Amine functionalized polyglycerols obtained by copolymerization of cyclic carbonate monomers, *Polymer*, 2018, **151**, 250–260.

36 K. Q. Li, X. L. Liu, L. Chen, Z. C. Xiong, C. D. Xiong and D. L. Chen, Synthesis of new aliphatic poly(ester-carbonate)s bearing amino groups based on photolabile protecting group and evaluation of antibacterial property, *Polym. Adv. Technol.*, 2022, **33**(4), 1100–1108.